Calculated electronic and optical properties of a graphite intercalation compound: LiC_6

1997 J. Phys.: Condens. Matter 9 9845

(http://iopscience.iop.org/0953-8984/9/45/012)

J. Phys.: Condens. Matter **9** (1997) 9845–9852. Printed in the UK PII: S0953-8984(97)83033-0

Calculated electronic and optical properties of a graphite intercalation compound: LiC_6

R Ahuja†, S Auluck‡, O Eriksson† and B Johansson†

† Condensed Matter Theory Group, Department of Physics, Uppsala University, Box 530, S-751 21, Uppsala, Sweden

‡ Department of Physics, University of Roorkee, Roorkee-247 667, India

Received 3 April 1997

Abstract. We have used the linear muffin-tin orbital method, without geometrical approximations, to calculate the electronic structure of LiC_6. Using our self-consistent solution, we have calculated the anisotropic frequency-dependent dielectric function and the reflectivity spectrum. The calculated reflectivity spectrum is in good agreement with the experimental data.

1. Introduction

Graphite is known to have many technological applications and has been the subject of intensive research both theoretically as well as experimentally. Hexagonal graphite has a c/a axial ratio of 2.7259 which gives rise to highly anisotropic electronic properties. Due to this circumstance graphite is often considered as a prototype system for layered crystals, showing essentially a two-dimensional behaviour. The carbon atoms within the basal plane are bound together by strong covalent σ-bonds (the nearest-neighbour distance is 1.42 Å) while atoms in adjacent layers are weakly bound by van der Waals bonds. As a result it is easy to intercalate foreign atoms (mainly alkali metals) or molecules (e.g. $AlCl_3$) into graphite. The intercalation compounds formed in this way have many interesting properties [1], which arise from changes in the electronic structure due to the intercalation. These compounds are of particular interest due to their possible technological applications [2].

When graphite intercalated compounds (GIC) are formed, an exchange of electrons takes place between the intercalant layers and those of the host, generating ionic bonding between layers and creating highly mobile charge carriers in the graphite layers. These charge-transfer effects have been studied experimentally for sulphuric acid–graphite using neutron diffraction [3], and for LiC_6 [4], monolayer graphite on a NbC crystal [5] and the alkali GICs [6] using angle-resolved photoelectron spectroscopy. The low-temperature specific heat of some GICs has been measured and the electronic density of states at the Fermi level, DOS(E_F), is found to be about 30 times larger than that of graphite [7]. LiC_6 has been studied most extensively, by means of measurements of the specific heat [8], metallic reflection [9], anisotropic conductivity [9], and NMR [10] and Raman spectroscopy [11]. Recently the Fermi surface of $AlCl_3$–graphite has been studied using de Haas–van Alphen [12] experiments.

There are not very many electronic structure calculations available in the literature for the GICs. Extended Hückel calculations for KC_8 have been carried out by Inoshita, Nakao and

0953-8984/97/459845+08$19.50

Kamimura [13]. The charge transfer in sulphuric acid–graphite was studied by means of first-principles total-energy electronic structure calculations [3]. These calculations were done by means of *ab initio* pseudopotentials within the LDA formalism using the Hedin–Lundqvist exchange–correlation potential. The calculations were made tractable by considering the changes induced in the graphite layers solely as a result of charge transfer. No energy bands were reported. The photoelectron spectroscopy data have been explained using a modified version of the combined discrete variational method [14] of Painter and Ellis [15]. Although this is not a self-consistent calculation, the agreement with the experimental data is good, and to this day this approach has remained the basic theoretical method used for comparison with experiments. The Fermi surface of the GICs has been calculated using an interpolation scheme based on the LCAO method [14–16] as well as the simpler tight-binding (TB) model [17].

The understanding of the GICs rests heavily on the idea that it is the π-bands of each 2D layer of graphite which are being partially emptied/filled in donor/acceptor compounds in the intercalation process. The band calculation of Holzwarth et al [14] seems to lend credence to this idea and suggests that the 2D rigid-band model of intercalation provides a good zeroth-order approximation to the Fermi level properties of LiC_6. Modifications caused by band folding due to the periodic perturbation of the intercalation layers and caused by the interlayer intercalations of the graphite layer leading to c-axis dispersion are very significant. In the present work we present an *ab initio* electronic structure calculation for LiC_6 using the full-potential linear muffin-tin-orbital (FPLMTO) method with the purpose of throwing more light on the validity of the rigid-band model and the role of interlayer intercalations in explaining the electronic properties of LiC_6. Comparison with our own earlier calculation on graphite [18] helps to highlight the role of the intercalation with Li.

2. Details of the calculations

In order to study the electronic structure of LiC_6 we have used the FPLMTO method [19]. The calculations were based on the local-density approximation and we used the Hedin–Lundqvist [20] parametrization for the exchange and correlation potential. Basis functions, electron densities, and potentials were calculated without any geometrical approximation [19]. These quantities were expanded in combinations of spherical harmonic functions (with a cut-off $\ell_{max} = 8$) inside non-overlapping spheres surrounding the atomic sites (muffin-tin spheres) and in a Fourier series in the interstitial region. The muffin-tin sphere occupied approximately 50% of the unit-cell volume. The radial basis functions within the muffin-tin spheres are linear combinations of radial wave functions and their energy derivatives, computed at energies appropriate to their site, and principal as well as orbital atomic quantum numbers, whereas outside the muffin-tin spheres the basis functions are combinations of Neuman or Hankel functions [21, 22]. For sampling the irreducible wedge of the Brillouin zone we used the special-k-point method [23]. In order to speed up the convergence we have associated each calculated eigenvalue with a Gaussian broadening of width 10 mRyd.

2.1. Calculation of the dielectric function

The ($q = 0$) dielectric function was calculated in the momentum representation, which requires matrix elements of the momentum, $\boldsymbol{p}$, connecting occupied and unoccupied eigenstates. To be specific, the imaginary part of the dielectric function, $\varepsilon_2(\omega) \equiv \mathrm{Im}\,\varepsilon(\boldsymbol{q} = 0, \omega)$,

was calculated from [24]

$$\varepsilon_2^{ij}(\omega) = \frac{4\pi^2 e^2}{\Omega m^2 \omega^2} \sum_{knn'\sigma} \langle \boldsymbol{k}n\sigma | p_i | \boldsymbol{k}n'\sigma \rangle \langle \boldsymbol{k}n'\sigma | p_j | \boldsymbol{k}n\sigma \rangle f_{\boldsymbol{k}n}(1 - f_{\boldsymbol{k}n'}) \delta(e_{\boldsymbol{k}n'} - e_{\boldsymbol{k}n} - \hbar\omega). \quad (1)$$

In equation (1), e is the electron charge, m its mass, Ω is the crystal volume and $f_{\boldsymbol{k}n}$ is the Fermi distribution. Moreover, $|\boldsymbol{k}n\sigma\rangle$ is the crystal wave function corresponding to the nth eigenvalue with crystal momentum $\boldsymbol{k}$ and spin σ. With our spherical wave basis functions, the matrix elements of the momentum operator can be conveniently calculated in spherical coordinates and for this reason the momentum is written as $\boldsymbol{p} = \sum_\mu \boldsymbol{e}_\mu^* p_\mu$ [25], where μ is -1, 0 or 1, and $p_{-1} = (1/\sqrt{2})(p_x - \mathrm{i}p_y)$, $p_0 = p_z$ and $p_1 = (-1/\sqrt{2})(p_x + \mathrm{i}p_y)$ [26].

The evaluation of the matrix elements in equation (1) is done over the muffin-tin region and the interstitial region separately. The integration over the muffin-tin spheres is done in a way similar to what Khan [27] and Gasche [24] did in their calculations using the atomic sphere approximation (ASA). A full detailed description of the calculation of the matrix elements will be presented elsewhere [18].

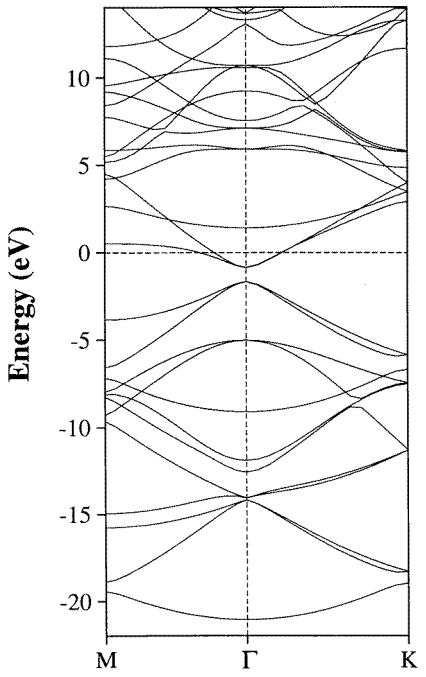

Figure 1. The calculated energy band structure of LiC_6 along the MΓK symmetry directions. The energy is in eV and the Fermi level (E_F) is set at zero energy.

The summation over the Brillouin zone in equation (1) is performed using linear interpolation on a mesh of uniformly distributed points, i.e. the tetrahedron method. Matrix elements, eigenvalues, and eigenvectors are calculated in the irreducible part of the Brillouin zone. The correct symmetry for the dielectric constant was obtained by averaging the calculated dielectric function. Finally, the real part of the dielectric function, $\varepsilon_1(\omega)$, is obtained from $\varepsilon_2(\omega)$ using the Kramers–Kronig transformation:

$$\varepsilon_1(\omega) \equiv \mathrm{Re}\big(\varepsilon(\boldsymbol{q} = 0, \omega)\big) = 1 + \frac{1}{\pi} \int_0^\infty \mathrm{d}\omega' \; \varepsilon_2(\omega') \Big(\frac{1}{\omega' - \omega} + \frac{1}{\omega' + \omega} \Big). \quad (2)$$

For a tetragonal or hexagonal structure we need to calculate two components of the total dielectric function [27], corresponding to light polarized parallel and perpendicular to the c-axis. In that case the total ε_2 is given by

$$\varepsilon_2^{tot}(\omega) = \frac{\varepsilon_2^{\parallel}(\omega) + 2\varepsilon_2^{\perp}(\omega)}{3} \tag{3}$$

where $\varepsilon_2^{\parallel}(\omega)$ and $\varepsilon_2^{\perp}(\omega)$ are the imaginary parts of the frequency-dependent dielectric function for the light polarized parallel and perpendicular to the c-axis.

Table 1. Characteristic energy levels (in eV) at the Γ point for graphite and LiC_6 relative to the Fermi energy.

	Graphite		LiC_6		
Symmetry label	Experiment	Theory[a]	Experiment[b]	Theory[c]	Theory[d]
π^*	0.0	0.0	−0.5	−1.3	−0.9, −1.7
$\sigma_{2,3}$	−4.6[b], 5.5[e]	−3.04	−5.0[g]	−5.9	−5.0
π_1	−7.2[b], −5.7[f],−6.6[e]	−6.52	−9.3	−9.3	−9.1
π_1	−8.1[b], −8.5[e]	−8.58			
$\sigma^*_{2,3}$	—	—	−13.0	−13.3	−12.6, −11.9
σ^*_1				−14.9	−14.0
σ^*_1, $\sigma^*_{2,3}$			−15.2	−15.4	−14.2
σ^*_1	−20.6[b]	−19.44	−22.5	−21.8	−21.1

[a] Ahuja *et al* [18].
[b] Eberhardt *et al* [4].
[c] Holzwarth *et al* [14].
[d] Present calculation.
[e] Law *et al* [28].
[f] Bianconi *et al* [29].
[g] This value is misprinted in table 1 of reference [4]. If we read this value from the corresponding figure, it is around 5.0 instead of 0.5.

3. Results and discussion

3.1. Band structure and the density of states

The band structure of LiC_6 has been calculated and is plotted in figure 1 along the MΓK direction (i.e. for $K_z = 0$). This band structure looks very similar to the one obtained by Holzwarth *et al* [14] using a modified version of the combined discrete variational method of Painter and Ellis [15]. However, these latter calculations were not self-consistent. One can get a good idea of the energy bands of LiC_6 from the graphite band structure by folding the LiC_6 BZ into the graphite BZ. Recall that the hexagonal unit cell of LiC_6 is three times the size of that of graphite. This has been explained very nicely by Holzwarth *et al* [14] for the two-dimensional carbon π-bands and we refer the reader to figure 4 of their article. This is in agreement with our own band structure near Γ. Our π-bands are split at Γ because they are 3D bands and not 2D ones. To make this comparison more quantitative, we list in table 1 values for some characteristic energy levels in LiC_6. These are compared with the calculation of Holzwarth *et al* [14] and experimental ARPEM data of Eberhardt *et al* [4].

Good agreement is obtained for all cases except for the $\sigma_{2,3}$- and π_1^*-bands which have been found by measurement to be degenerate 0.5 eV below E_F. Our calculation places the $\sigma_{2,3}$-band at 5 eV below E_F while Holzwarth *et al* [14] put it at 6 eV below E_F. We find the π_1^*-band at -0.9 and -1.7 eV below E_F whereas Holzwarth *et al* [14] put it at -1.3 eV. Our band structure shows clearly the splitting in the π_1^*- and $\sigma_{2,3}^*$-bands. This could be due to the fact that the FPLMTO method includes the interlayer scattering in the graphite structure in a more efficient way than the calculations of Holzwarth *et al* [14].

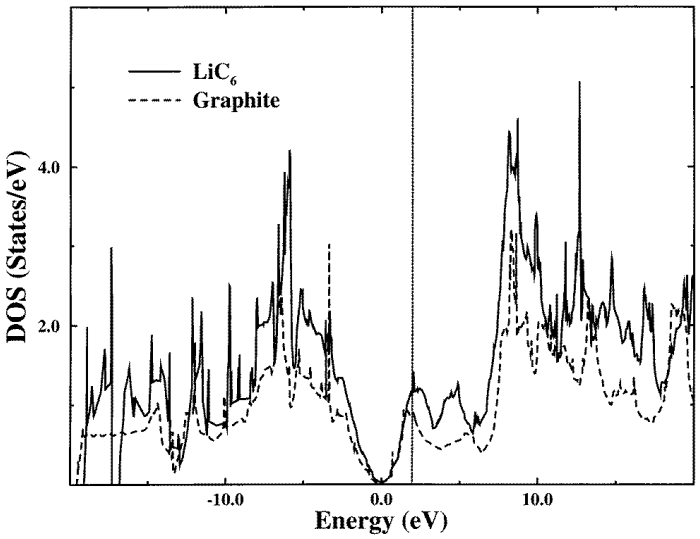

Figure 2. Calculated total densities of states (DOS) for LiC_6 and graphite. The Fermi level is set at zero energy for graphite. For LiC_6 it is marked by a vertical dotted line.

Graphite is semi-metallic with a very low density of states (DOS) at E_F. These states arise from the bands near the symmetry point K. In LiC_6 the presence of Li raises E_F (by contributing one conduction electron) thereby giving rise to a large DOS at E_F. We have plotted the DOS of LiC_6 in figure 2. This DOS is close to the DOS that we have previously calculated for graphite and shows 2D character. The major difference is the presence of a small peak above the Fermi energy for LiC_6. Moreover the Fermi energy is pushed to a higher energy than for graphite, in order to accommodate the extra 2s electron from Li. This picture of a direct transfer of the lithium electron into the graphite planes is further supported by the fact that at the minimum of the DOS (below E_F), the integrated number of electrons is 24, i.e. 4 electrons/C atom, while at E_F we have 25 electrons (one electron coming from Li 2s). The DOS at the minimum is 0.031 states eV^{-1} which gives 0.0051 states eV^{-1}/C atom. This should be compared to 0.0033 states eV^{-1}/C atom at E_F in graphite. The difference could well be explained by the folding of the BZ and hybridization. For LiC_6 we obtain the DOS at E_F, $D(E_F) = 1.17$ states eV^{-1}, which should be compared with the experimental value of 1.27 states eV^{-1} [8]. Holzwarth *et al* [14] obtained 1.44 states eV^{-1} which is somewhat larger than the experimental value. Using our value, the enhancement factor $(1+\lambda)$ comes out as 1.09 which is rather low and can thus help to explain why LiC_6 is not a superconductor. In contrast, a number of other graphite intercalation compounds have been found to be superconducting [13].

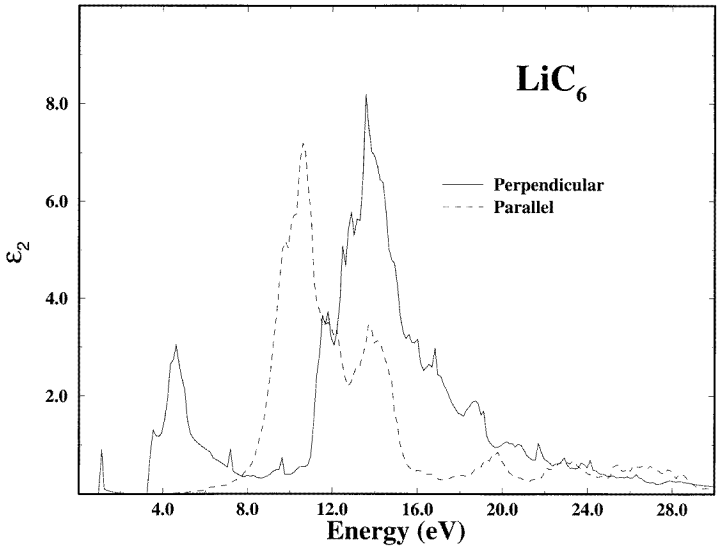

Figure 3. ε_2 calculated for LiC_6. 'Parallel' refers to the electric field parallel to the *c*-axis and 'Perpendicular' refers to the electric field perpendicular to the *c*-axis.

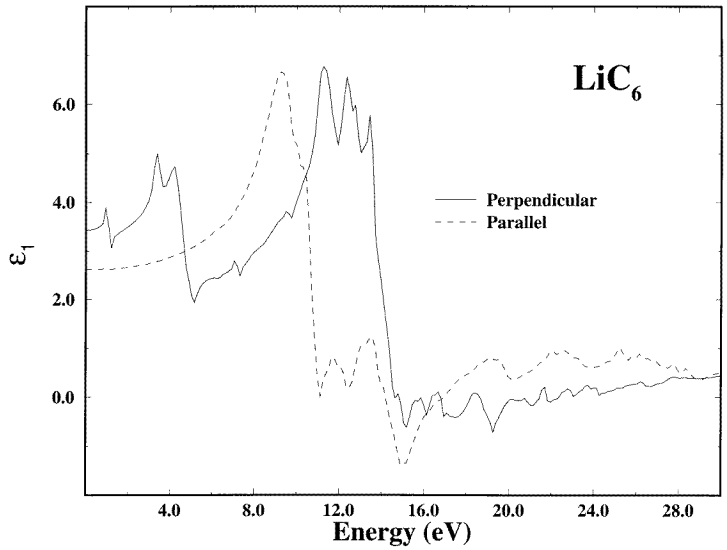

Figure 4. ε_1 calculated for LiC_6. 'Parallel' refers to the electric field parallel to the *c*-axis and 'Perpendicular' refers to the electric field perpendicular to the *c*-axis.

3.2. The optical response

We have calculated the anisotropic dielectric functions using the formalism mentioned earlier. In figure 3 we show the calculated behaviour of the interband $\varepsilon_2^{\parallel}(\omega)$ and $\varepsilon_2^{\perp}(\omega)$ functions. It is instructive to compare these with the corresponding results for graphite [18]. Consider first $\varepsilon_2^{\perp}(\omega)$. The two large peaks at around 1 and 4 eV for graphite show

up as relative peaks for LiC_6. However, the peak at 14 eV is present for both. As regards $\varepsilon_2^{\parallel}(\omega)$, the double-peak structure at 10 and 14 eV for graphite can be compared with the similar structure for LiC_6 while the low-energy weak structures for graphite are not found to be present for LiC_6. In our earlier paper on graphite [18] we attempted to link the various structures for $\varepsilon_2(\omega)$ to electronic transitions. This analysis will not be repeated here. Using Kramers–Kronig (KK) relations, we have calculated $\varepsilon_1(\omega)$. The results are plotted in figure 4. Because of the inherent problems with KK relations the $\varepsilon_1(\omega)$ is less accurate. Normally if $\varepsilon_2(\omega)$ is available up to say 3 Ryd, $\varepsilon_1(\omega)$ can only be relied upon up to 1 Ryd or so. Unfortunately no optical data for $\varepsilon_2(\omega)$ are available.

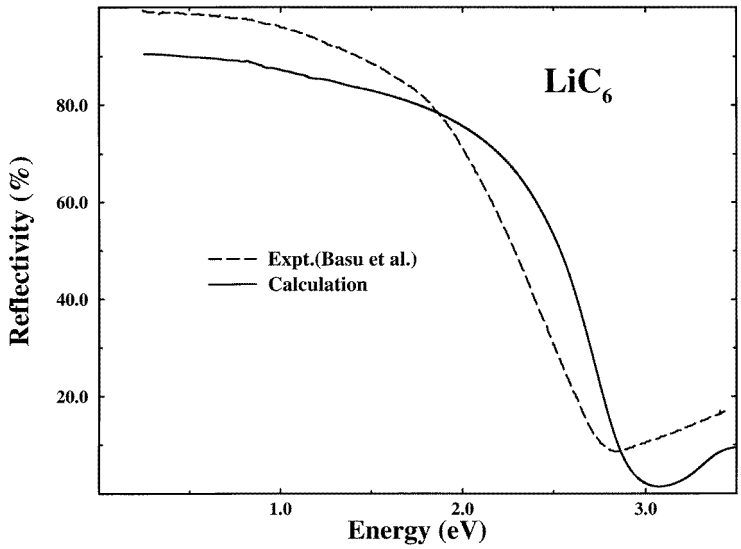

Figure 5. The calculated and experimental reflectivity for LiC_6. The experimental data are taken from Basu *et al* [9].

Using our calculated $\varepsilon_1(\omega)$ and $\varepsilon_2(\omega)$ we can calculate the reflectivity, and this is shown in figure 5. Also shown are the experimental data of Basu *et al* [9]. As can be seen, the agreement is good. The main difference is the location of the minimum, which is observed experimentally at 2.8 eV while it appears at 3.2 eV in our calculations.

4. Conclusions

We have calculated the electronic structure of the simple lithium-intercalated graphite compound LiC_6 using the FPLMTO method. A number of energy band features as well as structures in the DOS of LiC_6 can be related to similar features of graphite, but with the difference that E_F is pushed upwards to accommodate the one 2s electron of Li. Thus LiC_6 is not semi-metallic in character, in sharp contrast to graphite. Our calculations seem to suggest that Li does not play a very significant role except as a donor of an electron to the carbon network. A large discrepancy exists as regards the $\sigma_{2,3}$-band when we compare our eigenvalues with those deduced from the ARPEM data. The calculated interband $\varepsilon(\omega)$ is similar to our previous calculation for graphite except that a low-energy structure is lost. Unfortunately there are no experimental data available for LiC_6. However, our calculated reflectivity is in agreement with the experiment [9].

Acknowledgments

We wish to thank the Swedish Natural Research Council and the Materials Consortium No 9 for financial support and J M Wills for letting us use his FPLMTO code. One of us (SA) would like to thank the Condensed Matter Theory Group at Uppsala University for their kind hospitality.

References

[1] Zabel H and Solin S A (ed) 1990 *Graphite Intercalation Compounds I (Springer Series in Material Sciences 14)* (Berlin: Springer)
[2] Fischer J E and Thompson T E 1977 *Phys. Today* **30** 81
Fischer J E and Thompson T E 1978 *Phys. Today* **31** 36
[3] Chan C T, Kamitakahara W A, Ho K M and Eklund P C 1987 *Phys. Rev. Lett.* **58** 1528
[4] Eberhardt W, McGovern L T, Plummer E W and Fischer J E 1980 *Phys. Rev. Lett.* **44** 200
[5] Hwang Y, Aizawa T, Hayami W, Otani S, Ishizawa Y and Park S J 1992 *Solid State Commun.* **81** 397
[6] Oelhafen P, Pfluger P, Hauser E and Guntherodt H J 1980 *Phys. Rev. Lett.* **44** 197
[7] Mizutani U, Kordow T and Massalski T B 1978 *Phys. Rev.* B **17** 3165
[8] Delhaes P, Rouillon J C, Manceau J P, Guerard D and Herold A 1976 *J. Physique Lett.* **37** L127
[9] Basu S, Zeller C, Flanders P J, Fuerst C D, Johnson W D and Fischer J E 1979 *Mater. Sci. Eng.* **38** 275
[10] Conard J and Estrade H 1977 *Mater. Sci. Eng.* **31** 173
[11] Zanini M, Ching L Y and Fischer J E 1978 *Phys. Rev.* B **18** 2020
[12] Chien T R, Marchesan D, Ummat P K and Datars W R 1994 *J. Phys.: Condens. Matter* **6** 3031
[13] Inoshita T, Nakao K and Kamimura H 1977 *J. Phys. Soc. Japan* **43** 1237
[14] Holzwarth N A W, Rabii S and Girifalco L A 1978 *Phys. Rev.* B **18** 5190
Holzwarth N A W, Rabii S and Girifalco L A 1978 *Phys. Rev.* B **18** 5206
[15] Painter G S and Ellis D E 1970 *Phys. Rev.* B **1** 4747
Painter G S 1973 *Phys. Rev.* B **7** 3520
[16] Holzwarth N A W 1980 *Phys. Rev.* B **21** 3665
[17] Blinowski J, Hau N H, Rigaux C, Le Vieren J P, Toullee R, Furdin G, Herold A and Melin J 1980 *J. Physique* **41** 47
[18] Ahuja R, Auluck S, Wills J M, Alouani M, Johansson B and Eriksson O 1997 *Phys. Rev.* B **55** 4999
[19] Wills J M, unpublished
Wills J M and Cooper B R 1987 *Phys. Rev.* B **36** 3809
Price D L and Cooper B R 1989 *Phys. Rev.* B **39** 4945
[20] Hedin L and Lundqvist B I 1971 *J. Phys. C: Solid State Phys.* **4** 2064
[21] Andersen O K 1975 *Phys. Rev.* B 12 3060
[22] Skriver H L 1984 *The LMTO Method* (Berlin: Springer)
[23] Chadi D J and Cohen M L 1973 *Phys. Rev.* B **8** 5747
Froyen S 1989 *Phys. Rev.* B **39** 3168
[24] A good description of the calculation of dielectric constants and related properties is found in
Gasche T 1993 *Thesis* Uppsala University
[25] Edmonds A R 1974 *Angular Momentum in Quantum Mechanics* (Princeton, NJ: Princeton University Press) p 82
[26] In practice we calculate matrix elements of the symmetrized momentum operator $\langle i|\mathbf{p}_\mu|j\rangle \equiv (\langle i|p_\mu j\rangle + (-1)^\mu\langle p_{-\mu}i|j\rangle)/2$.
[27] Khan M A 1993 *J. Phys. Soc. Japan* **62** 1682
Khan M A 1993 *Appl. Surf. Sci.* **65** 18
[28] Law A R, Bary J J and Hughes H P 1983 *Phys. Rev.* B **28** 5332
[29] Bianconi A, Hagström S B M and Bachkrach R Z 1977 *Phys. Rev.* B **16** 5543